Journal of
Intelligent Material
Systems and Structures

Original Article

Journal of Intelligent Material Systems and Structures
2014, Vol. 25(13) 1644–1653

DOI: 10.1177/1045389X13510220
jim.sagepub.com
SAGE

A new deformation monitoring method for a flexible variable camber wing based on fiber Bragg grating sensors

Peng Li[1], Yanju Liu[2] and Jinsong Leng[1]

Abstract

This work presented an indirect method to monitor the deformation of the flexible variable camber wing using attached fiber Bragg gratings. To measure the transverse strains resulting from deformation of flexible variable camber wing, two groups of fiber Bragg grating sensors were attached on both upper and lower surfaces of the metal sheet, which was used to replace the traditional hinges. When the flexible variable camber wing was actuated by the lower surface's pneumatic artificial muscle actuators, the upper surface would undergo the tensile deformation. A redshift could be observed from the reflective wavelength of the fiber Bragg grating sensors located on the upper surface. On the contrary, a blueshift could also be observed from the lower surface due to the compressive deformation. The comparison of the results with those obtained from strain gauges demonstrated the reliability of fiber Bragg grating sensors. Then, the vertical displacement and deflection angle of the flexible variable camber wing were obtained through the von Karman strain–displacement relation. A finite element model of the flexible variable camber wing was developed to simulate the variation of strain and displacement, which is caused by deformation of the metal sheet. A good agreement could be seen from the vertical displacements among the fiber Bragg grating strain sensors, finite element model, and direct measurements with laser range-finders.

Keywords

Flexible variable camber wing, fiber Bragg grating sensors, finite element model, deformation monitoring

Introduction

With the development of the performance requirements of modern aerospace structures, the morphing aircraft (Barbarino et al., 2011) has shown the potential to greatly improve flight performance by changing the wing shape to adapt to the different flying situations and environment. The wing camber is the critical element comparing with other parameters for the wing to generate lift. Based on different requirements in different flight phases, states, and missions for aircraft's wing camber, the concept of variable camber wing had been proposed (Hardy, 1983). Considering structural safety and performance control, except for affecting the aerodynamic performance of wing flight, real-time and dynamic monitoring of the deformation of the morphing wings is essential in the deformation process. Conventional variable camber wing achieves the deflection using a mechanical hinge due to the limitations of the structural materials and design technology; the deflection angle of the trailing edge can be measured by the angle sensor. The rapid development of smart materials and structure technology promotes the realization of flexible variable camber wings (FVCWs) (Bil et al., 2013; McGowan et al., 2003; Sofla et al., 2010), which overcome the hinge devices' shortcomings, such as being heavy, complex, and inefficient. Experiments indicated that these new FVCWs (Barbarino et al., 2011) can further increase the lift–drag ratio and improve mobility, flight performance, and flow

[1]Centre for Composite Materials and Structures, Science Park of Harbin Institute of Technology (HIT), No. 2 YiKuang Street, P.O. Box 3011, Harbin 150080, People's Republic of China.
[2]Department of Aerospace Science and Mechanics, Harbin Institute of Technology (HIT), No. 92 West Dazhi Street, P.O. Box 301, Harbin 150001, People's Republic of China

Corresponding author:
Jinsong Leng, Centre for Composite Materials and Structures, Science Park of Harbin Institute of Technology (HIT), No. 2 YiKuang Street, P.O. Box 3011, Harbin 150080, People's Republic of China.
Email: lengjs@hit.edu.cn

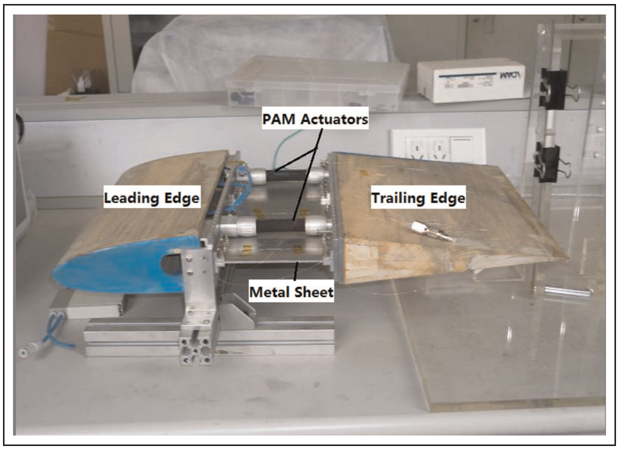

Figure 1. Photograph of FVCW's model without outer skin. FVCW: flexible variable camber wing; PAM: pneumatic artificial muscle.

separation. However, the previous angle sensors could not be applied to measurements during the operation of the new FVCWs, which do not contain the rotating structures.

When monitoring the shape deformation, the traditional direct measurement method generally used the noncontact optic method, which could be realized in the whole field structure measurement (Anand et al., 2009; Babovsky et al., 2011; Chan et al., 2009). But these methods are likely to be complicated and all have their limitations in the measurement environment. A possible approach is the measurement of other physical properties such as accelerations or strains, which can be measured using attachable sensors. The electrical resistance strain gauges have been used to sense the shape of the adaptive wing by Akl et al. (2007). Nishio et al. (2010) used Brillouin scattering–based optical fiber sensors for structural shape reconstruction. Rapp et al. (2009) and Reich and Sanders (2003) investigated the reconstruction method of structural deformation of two-dimensional structures by using a displacement–strain transformation matrix and Bragg grating sensors. However, all these methods require complex algorithms and models to measure the shape deformation and are not suited to the FVCW's situation in this work.

The objective of this work is to monitor the deflection angle and vertical displacement of an FVCW actuated by the pneumatic artificial muscles (PAMs) through strain measurement using attached strain sensors. Because of the advantages of fiber Bragg grating (FBG) sensors, such as nonvisual detection, small size, real-time distributed, multitask/point measurements, dynamic, antimagnetic, light, and other interference, they are used in a growing range of structural health monitoring applications (Fernando et al., 2003; Kiddy et al., 2005; Lima et al., 2008; Wu et al., 2009), especially in aerospace strain measurement (Kahandawa et al., 2012; Takeda et al., 2007; Wood et al., 2000; Yin et al., 2009b). In this work, the vertical displacement of the FVCW was monitored using a displacement–strain transformation through strain measurements from two couple-attached FBG sensors within one fiber optic line. Several simulations were made to investigate the sensor locations and to prove the correctness of the indirect method in theory. Furthermore, the measured structural displacements using laser range-finders showed that the estimated displacements are feasible.

FVCW

The FVCW analyzed in this work was proposed by Yin et al. (2009a, 2010), which consists of the leading edge, the metal sheet, the flexible skin, and the trailing edge. When the FVCW is working, the leading edge is fixed and provides the necessary boundary conditions, and the other parts are linked together and deformed. The metal sheet was used to replace the traditional hinges and achieve smooth and continuous deformation process. The actuation is a pure bending produced by compression strain of the two attached PAMs. The photograph of FVCW model without outer skin is shown in Figure 1.

The deformation process of the FVCW can be described as follows: when the PAMs located in the lower surface of the metal sheet are pressurized with air, their contraction deformation will result in downward bending of the wing. On the contrary, when the PAMs located in the upper surface are pressurized with air, the trailing edge would bend upward with contraction deformation. In this work, only the first case was studied as shown in Figure 2. The deformation degree of the FVCW changed with the different output contraction forces. The maximum contraction ratio of the PAM could reach up to 20%. Output force of every PAM can be measured by load transducer when air is applied. Then, the output pressure on the metal sheet could also be derived in different conditions, as listed in Table 1. The deformation of FVCW can be measured by the equivalent deflection angle. Generally, the traditional flap's length is about 15% of the wing chord, so the FVCW's equivalent deflection angle could be given as equation (1)

$$\beta_E = \sin^{-1}\left(\frac{h_T}{0.15c}\right) \tag{1}$$

where h_T and c are vertical displacement of the edge and chord, respectively. Therefore, the deformation process could be predicted through monitoring the vertical displacement of the edge.

The lengths of chord and trailing edge of the FVCW model are 500 and 230 mm, respectively. The metal sheet (aluminum alloy) with dimensions 300 mm $\times$ 120 mm $\times$ 1 mm, elastic modulus of 70 GPa, Poisson's ratio of 0.33, and tensile strength of 80 MPa was used at room temperature in this work. The wood with the elastic modulus of 0.98 GPa and Poisson's ratio of 0.49

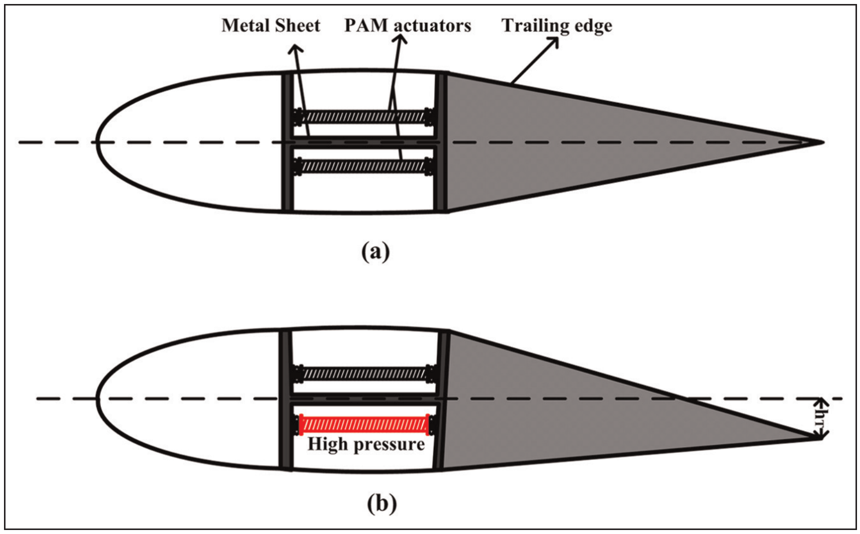

Figure 2. Schematic diagram of FVCW actuated by PAMs: (a) before deformation and (b) after deformation.
FVCW: flexible variable camber wing; PAMs: pneumatic artificial muscles.

Table 1. The average output pressure of PAM.

Input air pressure (MPa)	Average output force (N)	Average output pressure (MPa)
0.05	30	0.38
0.1	60	0.76
0.15	90	1.15
0.2	120	1.53
0.25	150	1.91
0.3	180	2.29
0.35	210	2.68
0.4	240	3.06

PAM: pneumatic artificial muscle.

was chosen as the material of the leading edge and trailing edge.

A three-dimensional finite element model (FEM) of the FVCW is shown in Figure 3. The FEM was conducted using ABAQUS. The FEM applied pressure and mesh of the FVCW are shown in Figure 3(a) and (b), respectively. The leading edge was constrained, and then, the metal sheet was applied in two pressures which are the same load to the PAMs' output force, thus the trailing edge created a vertical displacement. By applying different output pressures, the FEM changed the shape and performed some action, and then the displacement and strain field distributions of the FVCW were obtained. Taking a 0.2-MPa output pressure applied in PAM as an example, the specific vertical displacement and strain field distribution can be seen in Figure 3(c) and (d).The FEM predictions were correlated with strain/displacement measurement after applying air pressure loads to the FVCW.

In the measurement system, the number of sensors and their distribution should be optimized to minimize system complexity and cost based on the theoretical analysis while ensuring high measurement accuracy. Then, the trailing edge vertical displacement can be deduced by strain changes in the metal sheet. Therefore, the FBG sensors were only located on the metal sheet surfaces.

Theoretical approach

FBG sensing principle

FBG sensors' measurement principle is based on the detection of the back-reflected wavelength shift produced in an optical fiber whose core refraction index had been modulated permanently. According to grating theory, the Bragg wavelength or resonance condition of a grating is given by the expression (Kersey et al., 1997)

$$\lambda_B = 2n_{eff}\Lambda \tag{2}$$

where n_{eff} is the effective index of the core and Λ is the grating pitch.

The strain response arises due to both the physical elongation of the sensor (corresponding fractional change in grating pitch) and the change in fiber index due to photoelastic effects. The shift $\Delta\lambda_B$ in Bragg wavelength with strain $\Delta\varepsilon$ can be expressed using (Grattan and Meggitt, 1999)

$$\begin{aligned}\frac{\Delta\lambda_B}{\lambda_B} &= \left\{1 - \frac{n_{eff}^2}{2}[p_{12} - (p_{11} - p_{12})\upsilon]\right\}\Delta\varepsilon \\ &= (1 - p_e)\Delta\varepsilon = S_\varepsilon\Delta\varepsilon\end{aligned} \tag{3}$$

$$p_e = \frac{n_{eff}^2}{2}[p_{12} - (p_{11} - p_{12})\upsilon] \tag{4}$$

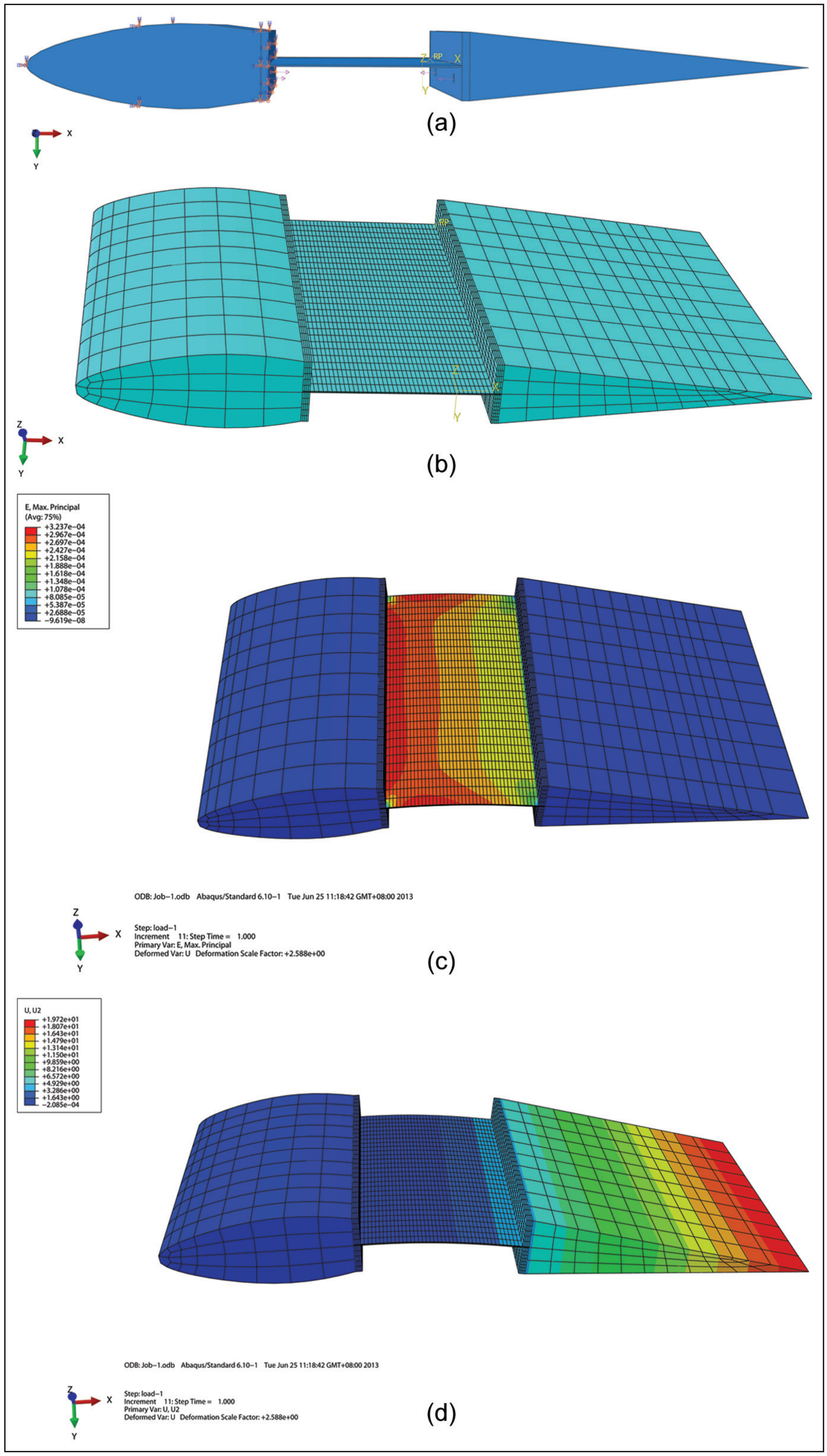

Figure 3. The finite element model of the FVCW: (a) the applied pressure, (b) the mesh model, (c) strain field distributions by 0.2 MPa pressure, and (d) displacement field distributions by 0.2 MPa pressure.
FVCW: flexible variable camber wing.

where p_e is the effective photoelastic constant, p_{11} and p_{12} are Pockle's (piezo) coefficients of the stress-optic tensor, and υ is Poisson's ratio

$$S_\varepsilon = 1 - p_e = 1 - \frac{n_{eff}^2}{2}[p_{12} - (p_{11} - p_{12})\upsilon] \tag{5}$$

where S_ε is the strain sensitivity coefficient of the FBG sensor.

Since the temperature change is neglected in the experiment process under laboratory conditions, the equation simplifies to

$$\varepsilon = \frac{1}{1 - p_e}\frac{\Delta\lambda_B}{\lambda_B} \tag{6}$$

It is easy to calculate the strain from the measured wavelength shift, and the value for a silica fiber responds linearly.

Displacement estimation method

The deformation of the FVCW was assumed under a vertical bending condition caused by PAM actuating. The objective of this study was to monitor the vertical displacement of the trailing edge in different air pressures by using FBG sensors as strain sensors. The von Karman equation could be used to describe strain–displacement relation. It is defined by

$$\varepsilon = u_{,x} + \frac{1}{2}(w_{,x})^2 - \eta w_{,xx} \tag{7}$$

where u and w are the axial and transverse displacements and η is the sectional vertical coordinate (positive downward). The length of the sensor i can be defined as L_i, and the strain measured by sensor i is the average range of the length and can be expressed as follows

$$\varepsilon_i = \frac{\Delta L_i}{L_i} = \frac{1}{L_i}\int_{x_i}^{(x_i + L_i)} \varepsilon dx = \frac{1}{L_i}\int_{x_i}^{(x_i + L_i)} \left[u_{,x} + \frac{1}{2}(w_{,x})^2 - \eta_i w_{,xx}\right]dx \tag{8}$$

The strain in the upper/lower surface of the metal sheet is expressed as

$$\varepsilon^U = u_{,x} + \frac{1}{2}(w_{,x})^2 + \frac{t}{2}w_{,xx} \tag{9}$$

$$\varepsilon^L = u_{,x} + \frac{1}{2}(w_{,x})^2 - \frac{t}{2}w_{,xx} \tag{10}$$

where superscripts U and L indicate upper and lower surfaces, respectively, and t is the thickness of the metal sheet.

Two sensors are located at the point 'x_i' on the upper and lower surfaces of the metal sheet, and the strain measured by sensor i can be expressed as

$$\varepsilon_i^U = \frac{\Delta L_i}{L_i} = \frac{1}{L_i}\int_{x_i}^{(x_i + L_i)} \varepsilon dx = \frac{1}{L_i}\int_{x_i}^{(x_i + L_i)} \left[u_{,x} + \frac{1}{2}(w_{,x})^2 + \frac{t}{2}w_{,xx}\right]dx \tag{11}$$

$$\varepsilon_i^L = \frac{\Delta L_i}{L_i} = \frac{1}{L_i}\int_{x_i}^{(x_i + L_i)} \varepsilon dx = \frac{1}{L_i}\int_{x_i}^{(x_i + L_i)} \left[u_{,x} + \frac{1}{2}(w_{,x})^2 - \frac{t}{2}w_{,xx}\right]dx \tag{12}$$

The difference in the above two equations can be expressed as

$$\left(\varepsilon_i^U - \varepsilon_i^L\right)L_i = t\int_{x_i}^{(x_i + L_i)} w_{,xx}dx \tag{13}$$

Equation (13) shows that this method eliminated the influences of the axial deformation and von Karman upon strain and avoided the iteration in solving process. It is supposed that the deflection curve of the sheet is polynomial of degree n. The deflection, rotation, and curvature can be expressed as follows

$$w = a_0 + a_1x + \cdots + a_nx^n \tag{14}$$

$$w_{,x} = a_1 + \cdots + na_nx^{n-1} \tag{15}$$

$$w_{,xx} = 2a_2 + \cdots + n(n-1)a_nx^{n-2} \tag{16}$$

Substituting equation (15) into equation (13) and integrating, the following can be obtained

$$\frac{\varepsilon_i^U - \varepsilon_i^L}{t} = 2a_2 + \cdots + na_n\frac{(x_i + L_i)^{n-1} - x_i^{n-1}}{L_i}(n \geq 2) \tag{17}$$

Based on the polynomial of degree 3 of the deflection curve, the strain expression is simplified as

$$\frac{\varepsilon_i^U - \varepsilon_i^L}{t} = 2a_2 + 3(2x_i + L_i)a_3 \tag{18}$$

There are two groups of the sensors at different locations at least because a_2 and a_3 are unknown. The resolution a_2 and a_3 can be given as follows

$$\begin{bmatrix} 2 & 3(2x_1 + L_1) \\ 2 & 3(2x_2 + L_2) \end{bmatrix}\begin{Bmatrix} a_2 \\ a_3 \end{Bmatrix} = \frac{1}{t}\begin{Bmatrix} \varepsilon_1^U - \varepsilon_2^L \\ \varepsilon_2^U - \varepsilon_2^L \end{Bmatrix} \tag{19}$$

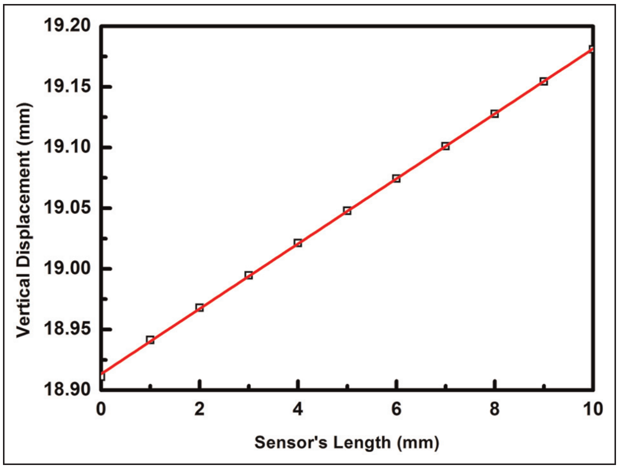

Figure 4. The vertical displacement against the different sensor's lengths (0.2 MPa).

Once the deflection of the metal sheet is computed, the vertical displacement of the edge can be easily determined using h_T as given by equation (20) and then the angular deflection can be computed from equation (1)

$$h_T = w|_{x=L} + (w_{,x}|_{x=L})L_{TE} \tag{20}$$

where L and L_{TE} are the length of the metal sheet and the length of edge, respectively.

Experimental details

Preparation of the FBG sensors

As shown in Figure 3(c), the strain distribution of the metal sheet along the axial direction is changed with large variation range. Therefore, it is necessary for choosing an appropriate length of the sensor for avoiding the spectra's split due to the nonuniform strain. In addition, the vertical displacement of the FVCW mainly depends on the strain of the metal sheet and almost has no relation to the sensor, but it can be seen that the parameter a_3's proof contains the length of the strain sensor from equation (18). If the length of the strain sensor is chosen appropriately, the obtained results could be more accurate for a given condition. In order to determine a reasonable sensor's length, an approximate method is used to estimate the minimum fiber length. For example, considering a given output air pressure (0.2 MPa), the vertical displacements were analyzed in terms of different sensor's lengths under certain conditions, as shown in Figure 4. The results indicated that the displacement was increased with the increasing sensor length. The measured vertical displacement would be more similar to the real vector as the length of the sensors is shortened. The reflection spectra of the short length grating will affect strain's measurement accuracy due to its broad bandwidth. Thus, 3 mm has been chosen as the attached FBG strain sensor's length.

The FBG sensors were ultraviolet (UV) inscribed in hydrogen-loaded standard fiber (SM-28) using a frequency-doubled Ar ion laser with the different standard phase mask scanning technique. Four FBG sensors were fabricated with almost 3 mm grating length using four kinds of phase masks along one optical fiber line, and their Bragg wavelengths are 1540.006nm, 1556.505nm, 1532.200nm, and 1535.300nm respectively. After the UV inscription, the FBGs were annealed at 80 °C for 48 h to stabilize their property at high working temperature. Finally, in order to maintain the durability, the stripped grating areas were recoated using acrylic resin. The FBGs' strain sensitivities were calibrated separately by tensile experiments. Their selected properties are presented in Table 2.

Experimental setup

According to the strain field distribution of the metal surface by FEM, the FBG sensors were distributed on the locations of movement with maximum amplitude for measuring strain accurately. Four different FBGs (1540.006, 1556.505, 1532.200, and 1535.300 nm) in a fiber line were divided into two groups, which were attached on the upper/lower surface of the metal sheet as shown in Figure 5.

External strain gauges were attached near the FBG sensors for comparing the results from the FBG sensors and the laser range-finder system for reference measurement to prove the method's feasibility. The whole experimental setup can be seen in Figure 6. The laser range-finders consisted of one laser sensor, controller unit, and a computer for data processing. The laser sensor was fixed above the trailing edge using a holder.

Table 2. Selected properties of the FBG sensors.

Sensor	Wavelength (nm)	Length (mm)	Strain limit ($\mu\varepsilon$)	Sensitivity $\left(\frac{pm}{\mu\varepsilon}\right)$
FBG_1	1540.006	3	3000	1.098
FBG_2	1556.505	3	3000	1.106
FBG_3	1532.200	3	3000	1.121
FBG_4	1535.300	3	3000	1.099

FBG: fiber Bragg grating.

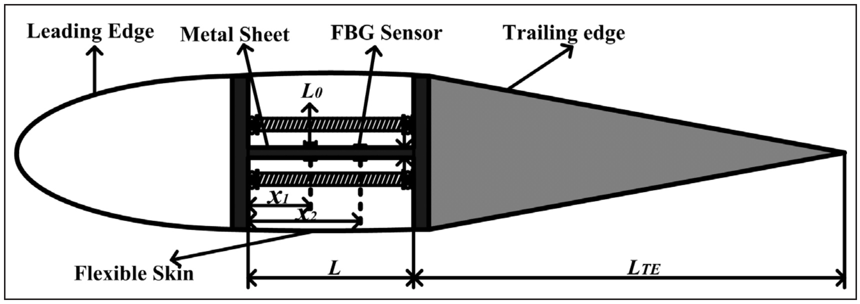

Figure 5. FBG strain sensors' arrangement diagram.
FBG: fiber Bragg grating.

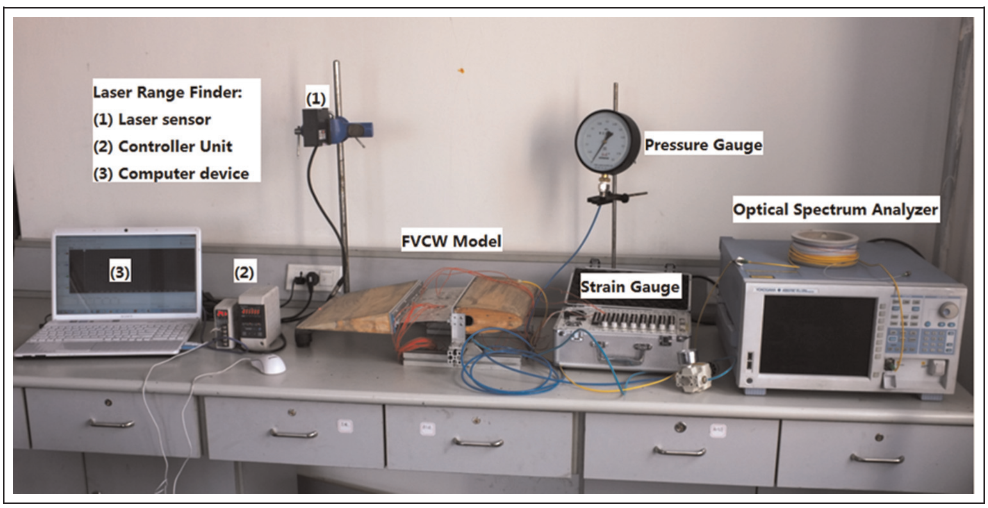

Figure 6. An FVCW model with four FBG sensors and kinds of measurement systems.
FVCW: flexible variable camber wing; FBG: fiber Bragg grating.

Only one channel was used to collect the strain data of four strain measurement points. First, the wavelengths of the FBG sensors can be obtained by the demodulation equipment. Second, the strain on the upper/lower surface of the metal sheet could be calculated according to the FBG's strain sensitivity. Finally, the vertical displacement of the trailing edge could be obtained using the strain–displacement transformation in section "Displacement estimation method" and the deformation of the trailing edge could be monitored.

Experimental results

The experimental and theoretical results for the strain of the metal sheet from different air pressures are plotted in Figure 7. Figure 7(a) and (c) represents the tensile strain measured on the upper surface, while Figure 7(b) and (d) shows the compressive strain measured on the lower surface of the sheet. From the curve line, it can be seen that the strains measured by the FBG sensors are in good agreement with those measured by the strain gauges. The theoretical predictions reveal that the strains measured by both FBG sensors and strain gauges are all lower than the numerical analysis results. Since the bonding method introduced a shear layer and reduced the measured strain, it is difficult to achieve the theoretical maximum, especially when bonding acrylate-coated fiber directly to a surface.

Good agreement between the FEM results and experimental response was observed for the four points of the FBG sensors. The experimental and theoretical investigation showed that the FBG sensors could be confidently used for measuring the strain of the metal sheet surface.

In order to achieve strain signal demodulation of the sensor and to obtain the vertical displacement of the FVCW, a simple computer program is designed for real-time displacement measurement. The program acquires the spectrum data from optical spectrum analyzer (OSA) or other spectrum analysis equipment first. And then, the data are divided into different groups according to the wavelength change trend. By choosing one peak of the curve and calculating its shift, the strain

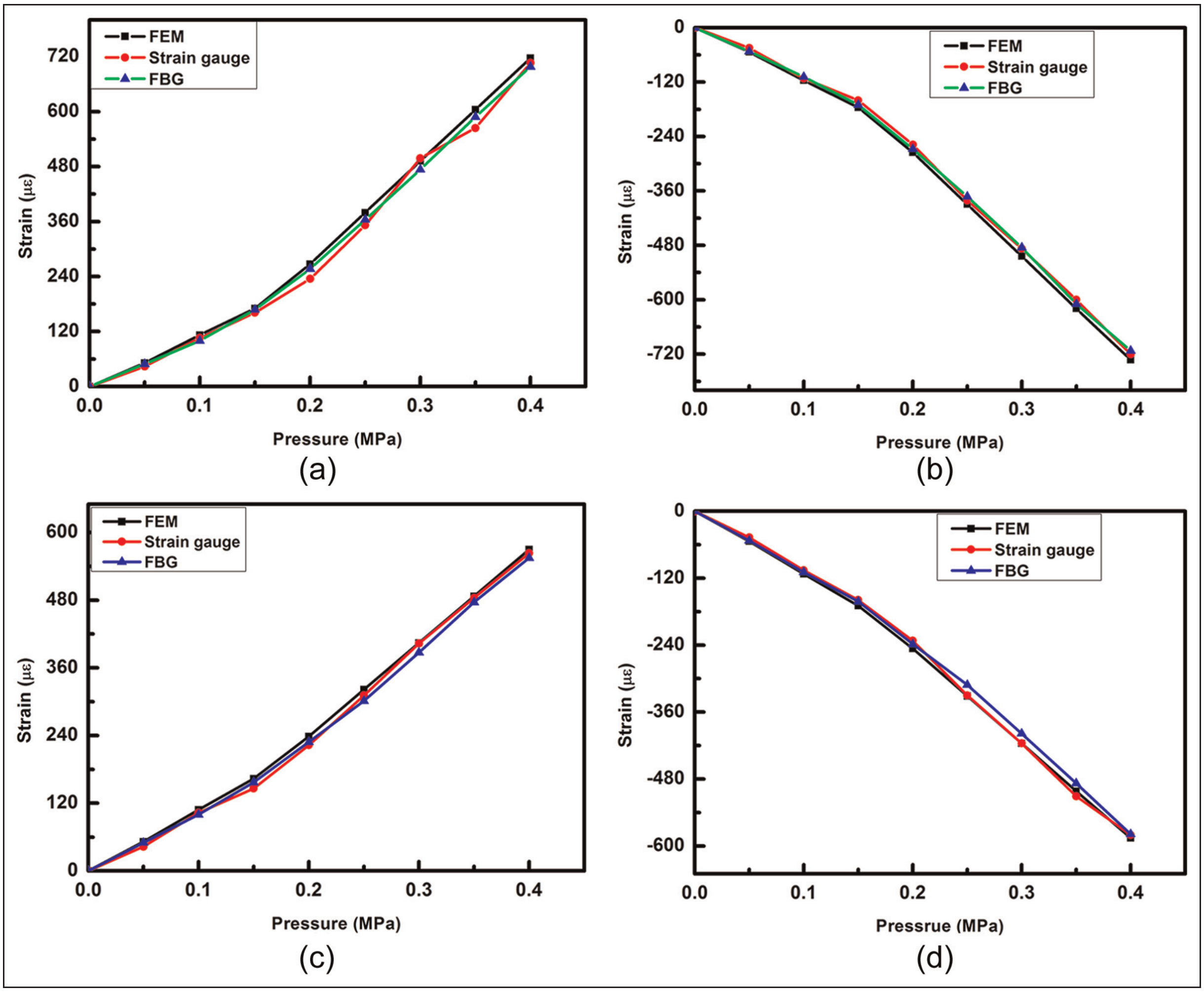

Figure 7. Comparisons of the strains analyzed by FEM and the strains measured by FBG sensors and external strain gauges at positions (a) x_1=50mm and (b) x_2=90mm on the upper surface, (c) x_1=50mm and (d) x_2=90mm on the lower surface.

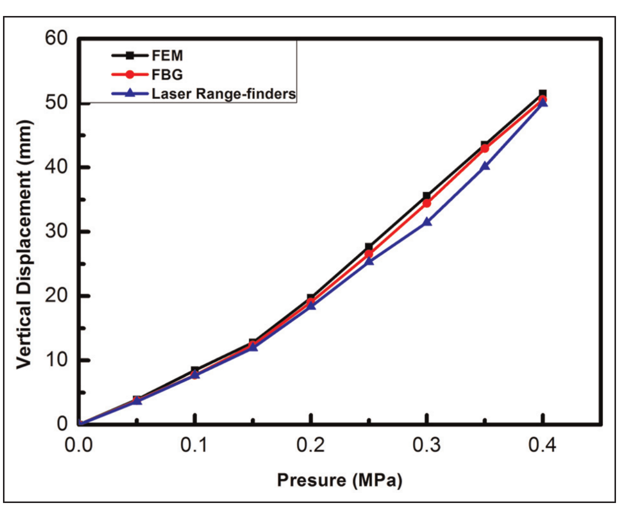

Figure 8. Comparisons of vertical displacement.
FEM: finite element model; FBG: fiber Bragg grating.

change can be demodulated according to equation (5). A series of the strain data at positions $x_1 = 50$ mm and $x_2 = 90$ mm were measured by the FBG sensors. Then substituting the strain data into equation (9), a_2 and a_3 were calculated. Finally, the vertical displacement could be obtained through equation (10), and the three group vertical displacements such as the FEM results, the direct measurements (using laser finder), and the deduced results (using the FBG sensor) were plotted and compared in Figure 8. The vertical displacement results obtained from the FBG strain sensors dovetailed well with FEM analysis results and the direct measurements using laser range-finders.

To evaluate the indirect method's feasibility and correctness using the quantitative results, where the results are shown in increasing pressure, the determined displacement errors are summarized in Figure 9. Figure 9(a) shows the theoretical errors between the

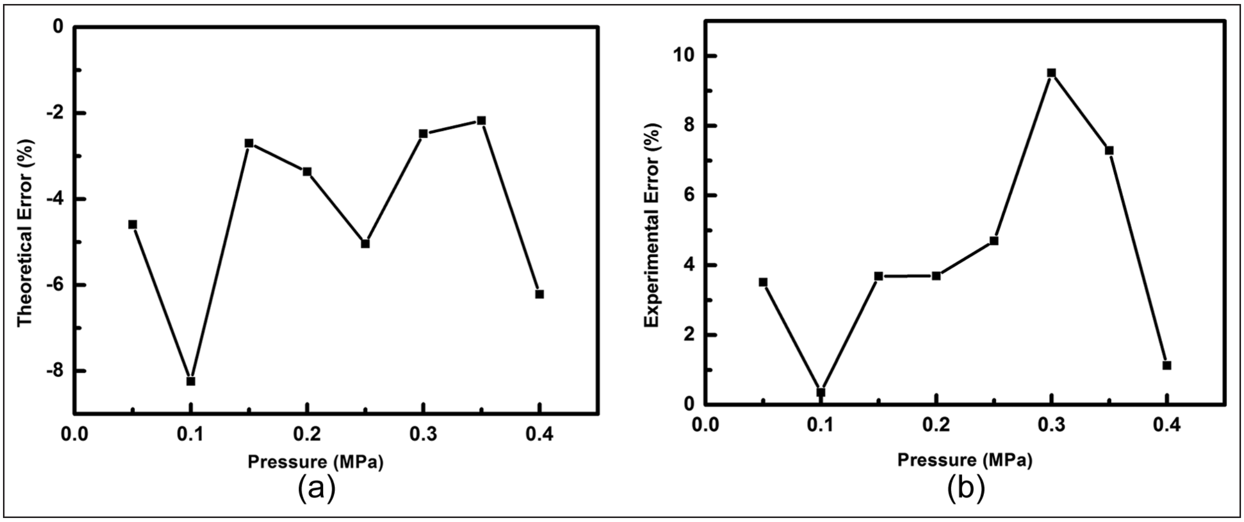

Figure 9. (a) Theoretical and (b) experimental errors regarding the output pressure.

FBG-calculated results and FEM results. As the strains of the metal measured by the FBG sensors are lower than the numerical analysis results, the FBG-calculated displacement results are smaller than the FEM results. Figure 9(b) shows the experimental errors between the FBG-calculated results and the direct measurements. Under the influence of gravity, air pump, and other actual practices, the FBG-calculated results are larger than the direct measurements. However, the average errors of the both average theoretical and experimental results under different air pressures are lower than 5%, which are all in the allowable range. They testify that the method adopted in this article is theoretically and experimentally feasible.

Conclusion

In this investigation, a new method for eliminating the influence of the axial deformation and the von Karman relation for monitoring the deformation are demonstrated. The developed theoretical model is validated experimentally using a flexible variable camber based on the change in strain provided with FBG. In comparison with the numerical results, the average errors are only around 5% in experiment and 3.5% in theory under different air pressures. The presented theoretical and experimental techniques have a significant impact on the safe deployment and effective operation of FVCW.

Declaration of Conflicting Interests

The authors declared no potential conflicts of interest with respect to the research, authorship, and/or publication of this article.

Funding

This work is supported by the National Natural Science Foundation of China (grant nos 11225211 and 11272106).

References

Akl W, Pohb S and Bazb A (2007) Wireless and distributed sensing of the shape of morphing structures. *Sensors and Actuators* 140: 94–102.

Anand A, Chhaniwal VK, Almoro P, et al. (2009) Shape and deformation measurements of 3D objects using volume speckle field and phase retrieval. *Optics Letters* 34: 10–12.

Babovsky H, Grosse M, Buehl J, et al. (2011) Stereophotogrammetric 3D shape measurement by holographic methods using structured speckle illumination combined with interferometry. *Optics Letters* 36: 23–25.

Barbarino S, Bilgen O, Ajaj RM, et al. (2011) A review of morphing aircraft. *Journal of Intelligent Material Systems and Structures* 22: 823–877.

Bil C, Massey K and Abdullah EJ (2013) Wing morphing control with shape memory alloy actuators. *Journal of Intelligent Material Systems and Structures* 24: 879.

Chan THT, Ashebo DB, Tam HY, et al. (2009) Vertical displacement measurements for bridges using optical fiber sensors and CCD cameras—a preliminary study. *Structural Health Monitoring* 8(3): 243–249.

Fernando GF, Hameed A, Winter D, et al. (2003) Structural integrity monitoring of concrete structures via optical fiber sensors: sensor protection systems. *Structural Health Monitoring* 2(2): 123–135.

Grattan KTV and Meggitt BT (eds) (1999) *Optical Fiber Sensor Technology*. *Volume 3—Applications and Systems*. Boston, MA: Kluwer Academic Publishers.

Hardy R (1983) AFTI/F-111 mission adaptive wing technology demonstration program. In: *Aircraft prototype and technology demonstrator symposium*, Dayton, OH, 23–24 March, paper no. 1057. Reston, VA: AIAA.

Lima HF, da Silva Vicente R, Nogueira RN, et al. (2008) Structural health monitoring of the Church of Santa Casa da Misericordia of Aveiro using FBG sensors. *IEEE Sensors Journal* 8(7): 1236–1242.

Kahandawa GC, Epaarachchi J, Wang H, et al. (2012) Use of FBG sensors for SHM in aerospace structures. *Photonic Sensors* 2(3): 203–214.

Kersey AD, Davis MA, Patrick HJ, et al. (1997) Fiber grating sensors. *Journal of Lightwave Technology* 15(8): 1442–1463.

Kiddy JS, Baldwin CS and Salter TJ (2005) Hydrostatic testing of a manned underwater vehicle using fiber optic sensors. In: *Proceedings of MTS/IEEE oceans conference*, Washington, DC, 17–23 September, pp. 1876–1881. New York: IEEE.

McGowan A-MR, Cox DE, Lazos BS, et al. (2003) Biologically-inspired technologies in NASA's morphing project. In: *Proceedings of SPIE, smart structures and materials: electroactive polymer actuators and devices*, San Diego, CA, 2 March, vol. 5051, pp. 1–13. Bellingham, WA: SPIE.

Nishio M, Mizutani T and Takeda N (2010) Structural shape reconstruction with consideration of the reliability of distributed strain data from a Brillouin-scattering-based optical fiber sensor. *Smart Materials & Structures* 19: 03501.

Rapp S, Kang L-H, Han J-H, et al. (2009) Displacement field estimation for a two-dimensional structure using fiber Bragg grating sensors. *Smart Materials & Structures* 18: 025006.

Reich GW and Sanders B (2003) Structural shape sensing for morphing aircraft. In: *Proceedings of SPIE, smart structures and materials: smart structures and integrated systems*, San Diego, CA, 2 March, vol. 5056, p. 134. Bellingham, WA: SPIE.

Sofla AYN, Meguid SA, Tan KT, et al. (2010) Shape morphing of aircraft wing: status and challenges. *Materials & Design* 31(3): 1284–1292.

Takeda S, Aoki Y, Ishikawa T, et al. (2007) Structural health monitoring of composite wing structure during durability test. *Composite Structures* 79(1): 133–139.

Wood K, Brown T, Rogowski R, et al. (2000) Fiber optic sensors for health monitoring of morphing airframes: I. Bragg Grating strain and temperature sensor. *Smart Materials & Structures* 9: 163–169.

Wu Z, Qing XP and Chang F-K (2009) Damage detection for composite laminate plates with a distributed hybrid PZT/FBG sensor network. *Journal of Intelligent Material Systems and Structures* 20: 1069–1077.

Yin W, Liu L, Chen Y, et al. (2009a) Variable camber wing based on pneumatic artificial muscles. In: *Proceedings of SPIE, second international conference on smart materials and nanotechnology in engineering*, Weihai, China, 8 July, vol. 7493, pp. 1–6. Bellingham, WA: SPIE.

Yin W, Liu L, Chen Y, et al. (2010) Pneumatic artificial muscle and its application on driving variable trailing-edge camber wing. *Proceedings of SPIE* 7292: 1–10.

Yin W, Fu T, Liu J, et al. (2009b) Structural shape sensing for variable camber wing using FBG sensors. In: *Proceedings of SPIE, sensors and smart structures technologies for civil, mechanical, and aerospace systems*, San Diego, CA, 8 March, vol. 7292, pp. 1–12. Bellingham, WA: SPIE.